

Modeling ϵ Eridani and asteroseismic tests of element diffusion

Ning Gai^{1,3}, Shao-Lan Bi^{2,1} and Yan-Ke Tang^{1,3}

¹ National Astronomical Observatories/Yunnan Observatory, Chinese Academy of Sciences, Kunming 650011, P. R. China

² Department of Astronomy Beijing Normal University, Beijing 100875, P. R. China

³ Graduate School of The Chinese Academy of Sciences, Beijing 100039, P. R. China

Abstract Taking into account the helium and metal diffusion, we explore the possible evolutionary status and perform seismic analysis of MOST target: the star ϵ Eridani. We adopt the different input parameters to construct the models by fitting the available observational constraints: e.g., T_{eff} , L , R , $[Fe/H]$. From computation, we obtain the average large spacings of ϵ Eridani about $194 \pm 1 \mu\text{Hz}$. The age of the diffused models has been found to be about 1 Gyr, which is younger than one determined previously by models without diffusion. We found that the effect of pure helium diffusion on the internal structure of the young low-mass star is slight, but the metal diffusion influence is obvious. The metal diffusion leads the models to have much higher temperature in the radiation interior, correspondingly the higher sound speed in the interior of the model, thereby the larger frequency and spacings.

Key words: stars: evolution — stars: interiors — stars: individual: ϵ Eridani

1 INTRODUCTION

Element diffusion, sometimes named “atomic” diffusion, is a basic physical element transport mechanism which is driven by pressure gradients (or gravity), temperature gradients and composition gradients. The effects of helium diffusion on the structure of solar models were first studied by Noerdlinger (1977). Later helioseismology provided an effective method to study this physical process (Guenther et al. 1993; Guenther 1994; Bahcall & Pinsonneault 1992b; Christensen-Dalsgaard et al. 1993; Guenther & Demarque 1997). Recently, helioseismic inferences have demonstrated that models incorporating element diffusion are in substantially better agreement with the inferred sound speed than the models that neglect it.

*E-mail: bisl@bnu.edu.cn; gaining@ynao.ac.cn

Up to date, the effect of element diffusion has been tested by asteroseismic method in solar type stars. According to the “second differences”, Vauclair & Théado (2004), Théado et al. (2005) and Castro & Vauclair (2006) presented discussion of asteroseismic signatures of pure helium diffusion in main-sequence stars between $1.1M_{\odot}$ and $2.0M_{\odot}$. In the present work, we study the effects of both helium and metal element diffusion on the models with mass less than $1M_{\odot}$.

Metal element could affect temperature gradient and convection in the envelope of stars. It also leads to the variations of the central temperature, density, pressure and radiative opacity. It is important to consider the influence of metal element on the internal structure of star. In this paper we mainly study the effects of metal diffusion on the stellar structure, evolution and the oscillation frequency for the late K-type star ϵ Eridani.

The bright K2V dwarf ϵ Eridani (HD22049, HIP16537, HR1084, PLX742) is one of the nearest solar-like stars, with a distance of about 3.218pc. It has a planetary companion ϵ Eridani b (Hatzes et al. 2000). Its proximity makes this planetary system as a prime target for future extrasolar planet direct – imaging efforts and studying the process of planetary systems formation. The success of these efforts will depend on the mass and the age of the system. Therefore the study of exoplanet – host star ϵ Eridani is a key issue.

In order to determine precise global parameters of the star ϵ Eridani, some authors performed numerous theoretical analysis (Guenther & Demarque 1986; Guenther 1987; Soderblom & Däppen 1989) (hereafter GD86, G87 and SD89 respectively). Thanked for Noyes et al. (1984), they measured the p -mode oscillation spectrum of ϵ Eridani and identified three individual frequencies in the power spectrum between $1500 \mu\text{Hz}$ and $2000 \mu\text{Hz}$ with average large spacing of $172 \pm 5 \mu\text{Hz}$. Based on non-asteroseismic and asteroseismic observational constraints, GD86, G87 and SD89 constructed a series of stellar models of ϵ Eridani. However, in their works for ϵ Eridani, there is a contradiction between the young age implied by the high chromospheric activity, rapid rotation rate, and the old age implied by the slightly metal-poor composition. In their works, GD86, G87 and SD89 discussed this contradiction and given the age 12 Gyr, 10 Gyr and 1 Gyr respectively.

Recently many evidences from observations seem to indicate that ϵ Eridani is a young main-sequence star with age less than 1 Gyr. For example, using Li abundances with the star’s position in the H-R diagram and kinematics, Song et al. (2000) derived the age of 0.73 ± 0.2 Gyr; Measuring the radius of ϵ Eridani by long-baseline interferometry, Di Folco et al. (2004) estimated the age at 0.85 Gyr; Saffe et al. (2005) used the calibrations of Donahue (1993) and Rocha-Pinto & Maciel (1998) (which corrected the age with an effect from chromospheric activity) to estimate the ages of 0.66 Gyr and 0.82 Gyr respectively. SIMBAD database describes the age of ϵ Eridani to be 0.66 Gyr.

The aim of present paper is to provide the basic theoretical studies of ϵ Eridani. We will use the latest interferometric observational radius (Di Folco et al. 2004) to constraint the stellar models and predict the frequency spacings. Then, we will investigate the effects of helium and metal diffusion on the internal structure, and the frequency spacings which also depend on the internal structure of the star.

In section 2, the global parameters of the star were summarized. The input physics, computing method and results analysis are summarized in section 3. The helium and metal diffusion effects on the stellar models, and the oscillation frequency are discussed in section 4. Finally, the conclusion is presented in section 5.

Table 1 The observational fundamental parameters of ϵ Eridani.

parameters	ϵ Eridani	Ref
M/M_{\odot}	0.85 ± 0.04	(1)
	0.80	(2)
	0.82	(3)
	0.83	(4)
$[Fe/H]_{surf}$	-0.13 ± 0.04	(5)
R/R_{\odot}	0.743 ± 0.010	(6)
M_v	6.18 ± 0.11	(7)
	6.18	(3)
$\log(L/L_{\odot})$	-0.4616 ± 0.044	(8)
$T_{eff}(K)$	5012 ± 67	(9)

(1)Santos et al. (2001); (2)Minier & Lineweaver (2006); (3)Takeda et al. (2005); (4)Fischer & Valenti (2005); (5)Santos et al. (2004); (6)Di Folco et al. (2004); (7)Song et al. (2000); (8)this paper; (9)Ramírez & Meléndez (2004)

2 OBSERVATIONAL CONSTRAINTS

Observationally it is difficult to determine accurately the mass of star except some binary systems. ϵ Eridani is a single star and it has various data of masses which were published in the literatures, for example $0.85 \pm 0.04M_{\odot}$ (Santos et al. 2001), $0.80M_{\odot}$ (Minier & Lineweaver 2006), $0.82M_{\odot}$ (Takeda et al. 2005), $0.83M_{\odot}$ (Fischer & Valenti 2005).

For the effective temperature of ϵ Eridani, we adopt $T_{eff} = 5012 \pm 67$ which was determined from the infrared flux method (IRFM) (Ramírez & Meléndez 2004).

The luminosity can be calculated using the absolute visual magnitude $M_v = 6.18 \pm 0.11$ (Song et al. 2000; Takeda et al. 2005). Given the bolometric correction $B.C. = -0.28$ (Takeda et al. 2005), the absolute bolometric magnitude is therefore $M_{bol} = M_v + B.C. = 5.9 \pm 0.11$. Then the luminosity is computed by formulae: $M_{bol} = -2.5\log(L/L_{\odot}) + M_{bol,\odot}$. Adopting $M_{bol,\odot} = 4.746$, we thus obtain $\log(L/L_{\odot}) = -0.4176 \sim -0.5056$.

ϵ Eridani is slightly metal-poor compared with the Sun. Santos et al. (2004) obtained $[Fe/H] = -0.13 \pm 0.04$ from the spectroscopic analysis basing on 39 Fe I and 12 Fe II lines. In order to deduce $[Z/X]$, we assume that the logarithmic value of $[Z/X]$ is proportional to the abundance ratio $[Fe/H]$ (Thoul et al. 2003):

$$\log[Z/X]_{star} = [Fe/H]_{star} + \log[Z/X]_{\odot} \quad (1)$$

where $[Z/X]_{\odot} = 0.023$ (Grevesse & Sauval 1998). Using this ratio, we obtain $[Z/X]_{surf} = 0.017 \pm 0.0016$.

A star's initial helium mass fraction Y_i is important for determining its structure, but Y_i of ϵ Eridani is unknown by observations. GD86, G87 adopted Y_i to be 0.236 and SD89 considered Y_i to be from 0.24 to 0.26. In our work, we reference the value given by GD86, G87, SD89 and adopt the initial helium abundance $Y_i = 0.245 \pm 0.015$.

The frequency, especially large spacings, sensitively depend on the radius. In order to predict the large spacings which will be observed by MOST, we take the latest interferometric observational radius $R/R_{\odot} = 0.734 \pm 0.01$ (Di Folco et al. 2004).

3 STELLAR MODELING

3.1 Input physics

The evolutionary models are computed using the Yale stellar evolution code version (Guenther et al. 1994) which has been modified to include the effects of element diffusion. The initial zero-age main sequence (ZAMS) models were calculated from pre-main sequence evolution which were assumed to have spherical symmetry, no rotation, no magnetic field. In the computation we use OPAL equation of state tables EOS2001 (Rogers & Nayfonov 2002), the opacities with a smooth blend of OPAL GN93 (Iglesias & Rogers 1996) and OPAL tables (Alexander & Ferguson 1994). The relevant nuclear reaction rates and cross sections are from Bahcall & Pinsonneault (1992a, 1992b) and Bahcall (1989). ϵ Eridani is a solar-like star, we choose the Krishna-Swamy (1966) atmosphere model. The diffusion of both helium and metal element abundance was considered in the stellar model computation, by using the coefficients of Thoul et al. (1994). In the next section we will introduce it in detail.

Using the standard mixing-length theory, we set $\alpha = 1.7$ for all models, close to the value which is required to reproduce the solar radius under the same physical assumptions and stellar evolution code (Murphy & Demarque 2004). If rotation and magnetic field are neglected in the construction of stellar model, convection is the most important mechanism that is usually included in standard stellar models which describes material motions within a star especially for low-mass main sequence star. The convective overshoot is another factor to influence the chemical composition of the star. The change of mixing-length parameter α would also influence principally the radius of the base of the external convection zone. The presence of core overshoot would extend the core-burning phase of evolution and increase the estimated age of star. This important topic has been studied separately by Bi et al. (2008). However, the element diffusion could also lead to the redistribution of the element in star and change the depth of the convective envelope (Guenther 1994). In order to test the effect of diffusion on the chemical composition, internal structure and the frequency of ϵ Eridani, we would not discuss the influence of the convection and overshoot in present work.

3.2 Element diffusion

The element diffusion in stars is driven by gravitational setting, temperature gradients, composition gradients and radiation pressure. It is described by Bahcall & Pinsonneault (1992a) in detail. The gravity and temperature gradients tend to concentrate the helium and heavier elements toward the center of the star, while the hydrogen diffuses outward. The concentration gradients oppose the above processes. In addition, radiation pressure can cause partially ionized or neutral species to rise relative to species with a small cross section. However, the radiation pressure are efficient in the external regions of main-sequence stars with $T_{eff} > 6000K$ (Michaud 1976). So the radiative pressure causes negligible diffusion in the K-type star and will be neglected in this paper.

3.2.1 Basic equation for element diffusion

Most works on chemical diffusion use either the Chapman - Enskog procedure (Chapman & Cowling 1970) or the method of Burgers (1969) for deriving the transport properties from the Boltzmann equation. In our work the element diffusion is described using the equations of Burgers (1969) with diffusion velocity

coefficients from Thoul et al (1994). A single model includes both helium and metal element diffusion. The change rate of the element mass fractions due to the diffusion is now written as (Thoul et al 1994; Bahcall & Loeb 1990):

$$\frac{\partial X_s}{\partial t} = -\frac{1}{\rho r^2} \frac{\partial [r^2 X_s T^{5/2} \xi_s(r)]}{\partial r} \quad (2)$$

where the partial derivatives are evaluated in the local rest frame of a mass shell in the star. ρ , r , T are the local value of density, radius, temperature and X_s is the mass fraction of element s .

The diffusion velocity for species s is defined by

$$w_s = \frac{T^{5/2} \xi_s}{\rho} \quad (3)$$

and the function $\xi_s(r)$ is expressed as

$$\xi_s(r) = A_p(s) \frac{\partial \ln p}{\partial r} + A_T(s) \frac{\partial \ln T}{\partial r} + \sum_{c \neq e, 2} A_c(s) \frac{\partial \ln C_c}{\partial r} \quad (4)$$

In equation (4), A_p , A_T , A_c correspond to gravitational settling, thermal diffusion and concentration gradient diffusion which are the functions of the mass fractions only. Species c can equal to s , but c aren't electron and helium element.

3.2.2 The treatment of diffusion in the evolutionary code

The Yale stellar evolution code has been modified to include the effects of He diffusion from gravitational settling and thermal diffusion (Bahcall & Pinsonneault 1992a) using the method of Bahcall & Loeb (1990) and added the metal diffusion in 1994. About the method by which treatment of element diffusion in a standard stellar evolution code, it has been described by Bahcall & Pinsonneault (1992a) in detail. In this section, we summarize it again.

In the diffusion subroutine written by Bahcall and Pinsonneault, the main problem is to solve the diffusion equation and calculate the change of the element abundance by diffusion. The diffusion equation (2) can be written as following form:

$$\frac{dx}{dt} = \frac{1}{\rho r^2} \left[\frac{d}{dr} (D_1) + \frac{d}{dr} (D_2 \frac{dx}{dr}) \right] \quad (5)$$

where D_1 , D_2 is the diffusion coefficients.

For helium diffusion

$$\begin{cases} D_1(Y) = \frac{F_{gy} \cdot r^2 \cdot T^{5/2}}{\ln \Lambda} \cdot \frac{d \ln p}{dr} \cdot X \cdot (A_p^X + A_T^X) \\ D_2(Y) = \frac{F_{gy} \cdot r^2 \cdot T^{5/2}}{\ln \Lambda} \cdot A_c^X \end{cases} \quad (6)$$

For metal diffusion

$$\begin{cases} D_1(Z) = \frac{F_{gz} \cdot r^2 \cdot T^{5/2}}{\ln \Lambda} \cdot \frac{d \ln p}{dr} \cdot Z \cdot (A_p^Z + A_T^Z) \\ D_2(Z) = \frac{F_{gz} \cdot r^2 \cdot T^{5/2}}{\ln \Lambda} \cdot A_c^Z \end{cases} \quad (7)$$

and radius, temperature, and density are in nondimensional units defined by $r = r'/R_\odot$, $T = T'/10^7 K$, $\rho = \rho'/100g \text{ cm}^{-3}$ and $t = t'/10^{13} \text{ yr}$ (Bahcall & Pinsonneault 1992a; Chaboyer et al. 1992).

In expressions (6) and (7), F_{gy} and F_{gz} are the adjustment factors by which the helium and metal diffusion coefficients are multiplied. In our work, we set

both of the two factors to 1.0. A_p , A_T , A_c are the diffusion velocity coefficients as described in equation (4). The exact numerical solution of these coefficients are calculated by an export subroutine which was developed by Thoul in 1994. The computation method is exhibited detailedly by Thoul et al. (1994).

In equation (5) the partial time derivative is evaluated at constant mass shell of the star. The diffusion equation is solved with zero hydrodynamic velocity of the stellar plasma. The right hand of diffusion equation (5) has two terms: the first term depends on first spatial derivatives of the element mass fraction and the second term depends on second spatial derivatives of the element abundance. The first term is solved explicitly using the two-step Lax-Wendroff technique (Press et al. 1986) by neglecting the second derivatives of the element abundance. We then use this trial solution as the initial abundance to determine the second derivatives by a fully implicit method (Bahcall & Pinsonneault 1992a). At last, the element abundance were updated.

For the helium diffusion, we only consider ^4He diffusion and ignore ^3He diffusion (Loeb et al. 1989). The time rate of change of the ^4He mass fraction Y is equal in magnitude and opposite in sign to the rate of change of the hydrogen mass fraction.

The diffusion of all metal elements were assumed to diffuse at the same rate as fully ionized iron. Because of the diffusion of metal elements, the radiative opacity have to be changed at each spherical shell in the stellar model after each time step. We calculate the effect of metal element diffusion on the opacity by computing a total metal element abundance at each model radius $Z(r)$, and then interpolating for the opacity between opacity tables with different total metal element abundances (Bahcall et al. 1995).

The diffusion subroutine carries out the diffusion calculations using data supplied by other parts of the Yale code, in which the thermal structure and the element abundances are calculated. It is assumed that the amount of diffusion within a given time step was too small to affect significantly the changes in thermal structure, in abundances, and in nuclear reaction rates that are calculated elsewhere. After the diffusion computation, we update the element abundance and then calculate the thermal structure.

In the diffusion subroutine, the element diffusion is treated only in the radiation region. The characteristic time for element to diffuse a solar radius under solar conditions is of the order of 10^{13} yr (Bahcall et al. 1995), much larger than the age of the sun and ϵ Eridani. However, helioseismic inferences have demonstrated the significance of the element diffusion (Cox et al. 1989; Bahcall & Loeb 1990; Bahcall & Pinsonneault 1992a; Proffitt 1994), we would test how much effect on the internal structure, the age and the frequency of ϵ Eridani by both the helium and metal diffusion using the asteroseismic method.

3.3 Computational method and results analysis

3.3.1 Evolutionary tracks and candidates for pulsation

In order to reproduce observational constraints of ϵ Eridani, we have computed a grid of evolutionary tracks for six masses M/M_\odot : 0.80, 0.81, 0.82, 0.83, 0.84, 0.85 and the initial metallicity Z_i : 0.011, 0.012, 0.013, 0.014.

From a series of evolutionary tracks which are computed, we select those models that land within the observational error box (being composed by $\log T_{eff}$, $\log L/L_\odot$, $\log R/R_\odot$) in the theoretical H-R diagram. Then we further choose the models on the basis of the constraint of the observational $[Z/X]$. In terms of the computation alone, we note that the age of ϵ Eridani is likely in

Table 2 Model Parameters of ϵ Eridani.

Model	A1	A2	A3	B1	B2	B3	C1	C2	C3
	$M/M_{\odot} = 0.83$ $Z_i = 0.012$ $Y_i = 0.2315$			$M/M_{\odot} = 0.83$ $Z_i = 0.013$ $Y_i = 0.2365$			$M/M_{\odot} = 0.83$ $Z_i = 0.014$ $Y_i = 0.2415$		
Dif.	None.	Y.Dif	Y& Z.Dif	None.	Y.Dif	Y& Z.Dif	None.	Y.Dif	Y& Z.Dif
Age(Gyr)	1.151	1.089	1.0	1.206	1.138	1.0	1.264	1.191	1.0
L/L_{\odot}	0.321	0.321	0.321	0.319	0.319	0.319	0.317	0.317	0.317
R/R_{\odot}	0.749	0.750	0.744	0.750	0.751	0.743	0.751	0.753	0.741
T_{eff}	5024.9	5019.8	5039.5	5012.2	5006.7	5036.3	4999.9	4993.8	5033.5
r_{cz}/R	0.7073	0.7053	0.7048	0.7046	0.7033	0.7024	0.7024	0.7022	0.7000
$\tau_{cz}(s)$	1504.8	1514.1	1496.7	1514.4	1522.9	1496.7	1523.2	1529.5	1497.0
$\tau_0(s)$	2524.5	2532.5	2502.4	2530.1	2538.8	2493.6	2535.7	2545.2	2484.5
$\tau_{cz}(s)/\tau_0(s)$	0.5961	0.5979	0.5981	0.5986	0.5999	0.6002	0.6007	0.6009	0.6025
$< \Delta\nu >$	192.2	191.4	193.8	191.6	191.0	194.6	191.2	190.5	195.1

the range 0.1 Gyr – 1.0 Gyr. Here we consider the age (≤ 1 Gyr) as a property of star which be same as SD89. According to the age estimation from observation, which given in the introduction, we constraint the age of models in the range 0.60 Gyr – 1.0 Gyr. At last, 12 tracks fall within the observational error box and are plotted in Fig. 1 (a).

In order to deduce the set of parameters lending to the better agreement with observations, we perform a χ^2 minimization method described by Eggenberger (2005). We define the χ^2 function as follows:

$$\chi^2 \equiv \sum_{i=1}^4 \left(\frac{C_i^{theo} - C_i^{obs}}{\sigma} \right)^2 \quad (8)$$

where the vector C_i^{obs} contains the observations: $C_i^{obs} \equiv (L/L_{\odot}, T_{eff}, R/R_{\odot}, [Z/H]_s)$. The value C_i^{obs} and the vector σ which contains the errors on the observations are given in Table 1. From this method we obtain three models A3, B3 and C3 which are given in Fig. 1 (b) and Table 2.

3.3.2 Calibration of models with and without diffusion

In order to investigate the effect of element diffusion, especially metal diffusion, basing on the selected models A3, B3 and C3, we calibrate three groups of models with mass $M/M_{\odot} = 0.83$. There are the different initial chemical compositions among the different groups. The models at the same group have the same initial chemical compositions, but they have different types of element diffusion. The detail description of the models are given in Table 2.

We use the stellar pulsation code of Guenther (1994) to calculate the eigenfrequencies and the large spacings of models listed in Table 2. For solar-like stars, the eigenfrequencies $\nu_{n,l}$ of oscillation modes, characterized by the radial order n at harmonic degree l , satisfy the simplified asymptotic relation (Tassoul 1980):

$$\nu_{n,l} = \Delta\nu \left(n + \frac{l}{2} + \alpha + \frac{1}{4} \right) + \epsilon_{n,l} \quad (9)$$

The large spacings is defined by the frequencies of the same harmonic degree l and the adjacent radial order n :

$$\Delta\nu_{n,l} \equiv \nu_{n,l} - \nu_{n-1,l} \quad (10)$$

We average the large spacings over the modes $l = 0, 1, 2, 3$ and $n = 10, 11, \dots, 30$ to obtain the average large spacings.

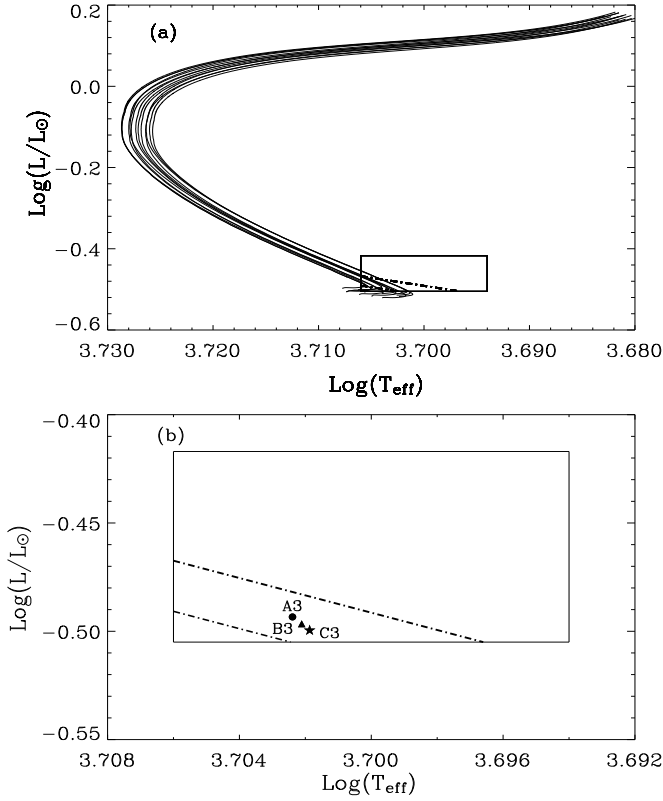


Fig. 1 (a) Evolutionary tracks (12 in total) in the H-R diagram from ZAMS. The solid lines indicate the boxes delimited by the observed luminosity and effective temperature. The two dash dot lines denote the boxes delimited by the interferometric radius. (b) Enlarge the error box of Fig (a). The model A3, B3 and C3 are denoted by filled circle, triangle and five pointed star respectively.

From the age of the star in Table 2, we can see that the diffusion could speed up the evolution of stars. The model with both helium and metal diffusion has the smallest age of all the models in the same group. The average large spacings is about $194 \pm 1 \mu\text{Hz}$ of models A3, B3 and C3. The pure helium diffusion hardly affect $\nu_{n,l}$, but the effect is relatively obvious after adding the metal diffusion. It also seems that the diffusion effect is increase along with the increase of the initial heavy element abundance (Y_i, Z_i). In the following section, we select models in group (C) to discuss differences in their internal structures in detail using the asteroseismic method.

4 ASTEROSEISMIC TEST HELIUM AND METAL DIFFUSION EFFECTS

4.1 “Second differences” tests helium and metal gradients

Stellar acoustic p -modes with low l degree can propagate deeply inside the stars. However, as mentioned by Gough (1990), rapid variations of the sound speed in-

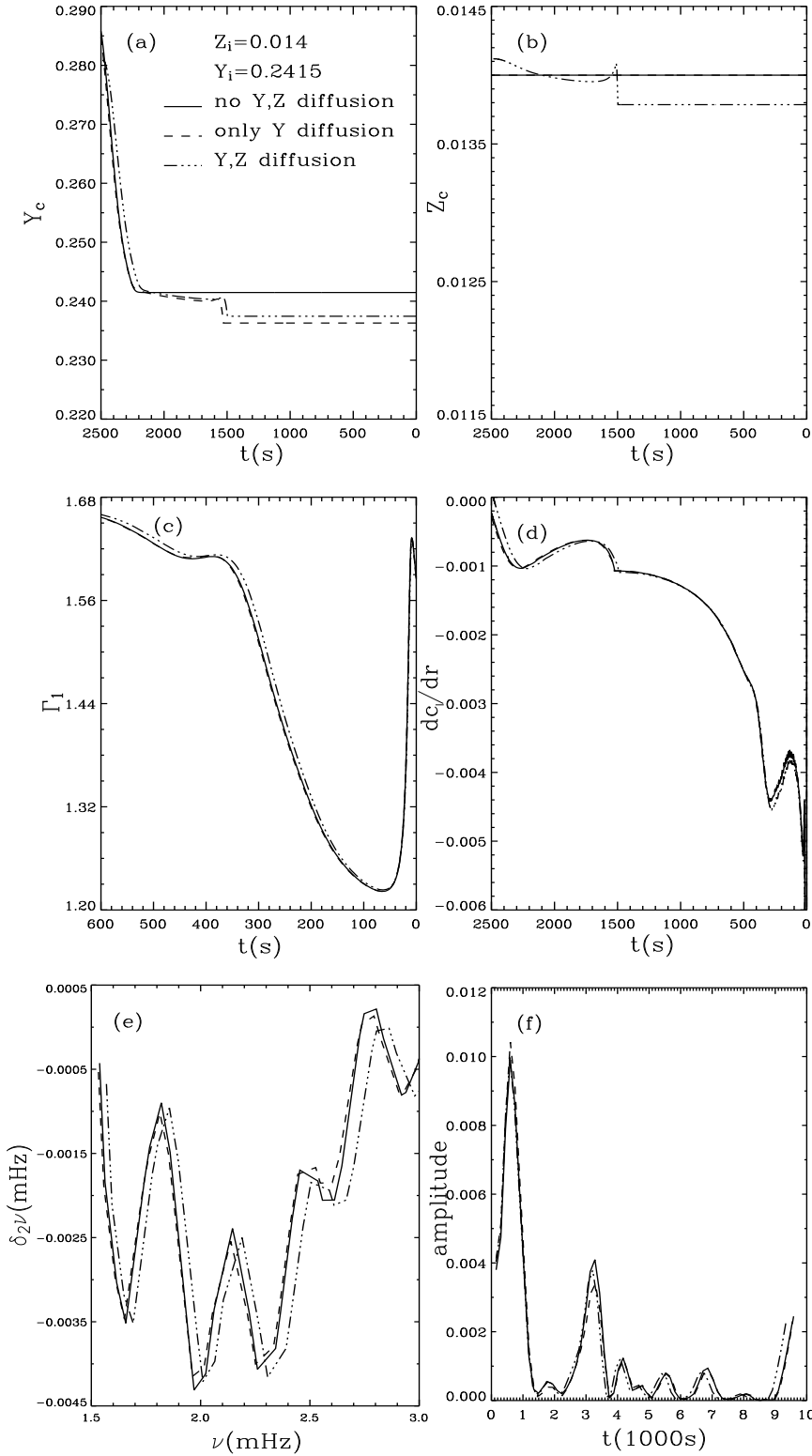


Fig. 2 The stellar structures of the group (C) models in Table 2 with $Y_i = 0.2415$, $Z_i = 0.014$. The detailed notes are labeled in the figure. Solid lines: standard homogeneous model C1 without diffusion; dashed lines: model C2 with pure helium diffusion; dash dot lines: model C3 with both helium diffusion and metal diffusion. The panel (a) helium profiles as a function of the acoustic depths in the models, i.e. the time for the acoustic waves to travel from the surface down to the considered layer; (b) the metal profiles: a clear gradient at the bottom of the convection zone; (c) the adiabatic exponent Γ_1 profiles which show a clear feature

side a star lead to partial reflections of the sound waves. A conveniently and easily evaluated measure of this oscillatory component is the “second differences” with respect to the radial order n of the frequencies ν_{nl} for the same value of the harmonic degree l :

$$\Delta_2\nu_{nl} \equiv \nu_{n-1,l} - 2\nu_{n,l} + \nu_{n+1,l} \quad (11)$$

This measure is contaminated less than the first difference $\Delta_1\nu_{nl} \equiv \nu_{n,l} - \nu_{n-1,l}$ by the smoothly varying components of $\Delta_1\nu_{nl}$. This modulation in the frequency has been extensively studied in the He_{II} ionization zone and the edge between the convective and radiative zones. In the He_{II} ionization zone there is a rapid variation of the adiabatic exponent Γ_1 and in the base of the convection zone there is essentially a discontinuity in the sound speed gradient, i.e. dc/dr , produce a discontinuity in ν_{nl} . In order to identify the different components which modulate the oscillations, we have computed the Fourier transform of the “second differences”. The modulation period of the “second differences” is twice the “acoustic depth” of the region where the feature occurs:

$$\tau_s = \int_{r_s}^R \frac{dr}{c(r)} \quad (12)$$

where τ_s is the time needed for the acoustic waves to travel between the surface and the considered region (the He_{II} ionization zone or the base of the convection zone), $c(r)$ is the sound speed at radius r , and r_s is the radius of the considered region.

Vauclair & Théado (2004), Théado et al. (2005) and Castro & Vauclair (2006) described asteroseismic signatures of pure helium diffusion in stars between $1.1M_\odot$ and $2.0M_\odot$ in terms of “second differences”. They have studied the precise signatures on the oscillation frequencies of helium gradients inside stars. In our work we compute stars of $0.83M_\odot$ in which not only including helium diffusion but also containing metal diffusion. The aim of the present section is to study the precise signatures on the oscillation frequencies of not only helium gradients but also metal gradients inside stars and to test the effect of metal diffusion on the internal structure.

Fig. 2(a)(b) display the helium and metal abundance profiles in the models without element diffusion (solid line), with pure helium diffusion (dashed line) and with both helium and metal diffusion (dash dot line) as a function of the acoustic depth. Due to diffusion, helium and metal drift inward and form a gradient just below the convective zone. The acoustic depth of the bottom of the convection zones τ_{cz} and the corresponding τ_{cz}/τ_0 , where τ_0 is the total acoustic depth of the star, are listed in Table 2 about models with different initial chemical composition and different types of diffusion. Fig. 2(c)(d) give the adiabatic exponent Γ_1 profiles and the sound speed gradients dc/dr versus the acoustic depth. From the dc/dr profiles it is clear to see that the dips around 300s and 1500s are caused by the He_{II} ionization zones and the bottom of the convection zones.

Considering the asymptotic approximation validity, we select modes of degrees $l = 0, 1, 2, 3$ and oscillation frequencies between $1500\mu Hz$ and $3000\mu Hz$ to compute the “second differences”. In Fig. 2(e)(f) we present the second differences of our models and the Fourier transforms of these curves. We have explained that the modulation period corresponding to the peaks in the Fourier transforms are twice the “acoustic depth” of the region where the feature occurs. By comparing the dips of dc/dr profiles in Fig. 2(d) with Fourier transforms in Fig. 2(f), one can easily recognize the peaks due to the He_{II} ionization zones and those due to the bottom of the convective zones in Fig. 2(f).

From the Fourier transforms in Fig. 2(f), we can see that the amplitudes of the peaks corresponding to the modulation periods due to the base of the convection zones of models C1, C2, C3 are different. Mazumdar & Antia (2001) shown that the amplitude of the oscillatory signal in the second differences contains an amplification factor of $4 \sin^2(\pi\tau_s/\tau_0)$. When $\tau_s/\tau_0 > \frac{1}{2}$, the Fourier transforms show the peak amplitudes decrease for deeper layers (Vauclair & Théado 2004). In terms of r_{cz}/R and τ_{cz}/τ_0 in Table 2, we find that diffusion could deepen the outer convective zone, especially including the metal diffusion, the base of the convective zone is deepest of all in the same group. From the Fourier transforms, we can see that the peak amplitude at $2\tau_{cz}$ of models with pure helium diffusion is lower than that without diffusion. In term of amplification factor of $4 \sin^2(\pi\tau_s/\tau_0)$, the peak amplitude of models with both helium and metal diffusion should be lowest of all, but it is higher than that with pure helium diffusion. So we think that the peak amplitude is mainly determined by the depth of the base of the convection zone, meanwhile it is also sensitive to the element gradient at the bottom of convective zone. From Fig. 2(b), it is clear to see that the metal gradient steepen more rapidly than helium gradient. There is a stronger reflection of the sound waves in the region of the metal gradient, that is why the model contain metal diffusion have a higher amplitude of the peak of τ_{cz} .

4.2 Tests of internal structure

In this section, we compute the so-called small frequency spacings and frequency separation ratios of the low- l p -modes to test the internal structure of models in which considered different types of diffusion. The small frequency spacings is given by the combination:

$$d_{l+2}(n) = \nu_{n,l} - \nu_{n-1,l+2} \quad (13)$$

Using the asymptotic theory of p modes it can be shown that (Christensen-Dalsgaard & Berthomieu 1991; Basu et al. 2007):

$$d_{l+2}(n) \simeq -(4l+6) \frac{\Delta\nu_{nl}}{4\pi^2\nu_{n,l}} \int_0^R \frac{dc}{dr} \frac{dr}{r} \quad (14)$$

where R is the stellar radius and $\Delta\nu_{nl}$ is the large spacings. In the core the gradient of the sound speed is large and r is small, the integral in equation (14) is dominated by conditions in the core. So the small spacings usually test the stellar core. But the small spacings are also slightly affected by near-surface effects. In order to reduce the effect of near surface uncertainties, the frequency separation ratios are used (Roxburgh & Vorontsov 2003):

$$r_{02}(n) = \frac{d_{02}(n)}{\Delta_1(n)}, \quad r_{13}(n) = \frac{d_{13}(n)}{\Delta_0(n+1)} \quad (15)$$

Each panel of Fig. 3 show small spacings d_{02} and frequency separation ratios r_{02} for different models in group (C) with different types of diffusion which are labeled in the figure. From the small spacings and frequency separation ratios we can see that the pure helium diffusion hardly alter the internal structure in these young low-mass models. By comparing the models included metal diffusion with the models no element diffusion, the differences of their internal structures are relatively obvious.

In order to explain the changes of the internal structure from the asteroseismic test, we compare the internal physical parameters of models with and

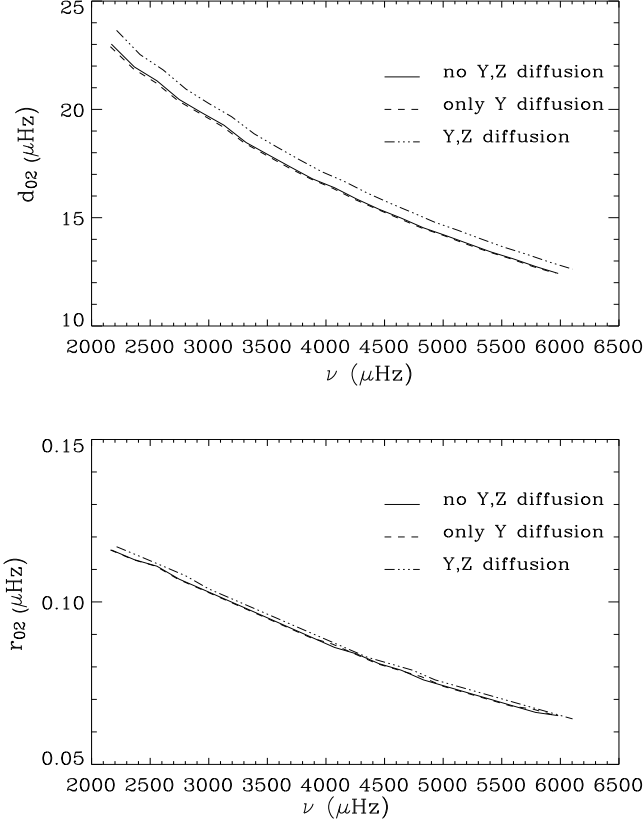


Fig. 3 Upper part: small spacings $d_{02}(n)$, lower part: frequency separation ratios $r_{02}(n)$ for the models in group (C). The detailed notes are labeled in the figure.

without diffusion. It is known that the sound speed depends on both the mean molecular weight and the temperature (Basu et al. 2007; Bi et al. 2008)

$$c^2 \simeq \frac{K_B T}{\mu m_u} \propto \frac{T}{\mu} \quad (16)$$

In Fig. 4, we give the $\delta c/c$, $\delta T/T$, and $\delta \mu/\mu$ variations as function of radius.

From Fig. 4, it is clear to see that the effect of the pure helium diffusion on the sound speed c , temperature T and the mean molecular weight μ is small. The helium diffusion hardly alter the c , T and μ in the radiation interior and the effect mainly concentrate on the convection zone. Due to diffusion, helium drift inward just below the convection zone. It induce μ is smaller than that without diffusion in the envelope. On the other hand, the increase of the opacity in the envelope due to the settling of He leads to the lower temperature than that without diffusion. However, the helium diffusion decrease both the T and μ , the sound speed c slightly in the convective envelope. So the small spacings and separation ratios are similar with and without helium diffusion.

In Fig. 4 the dash dot lines describe the differences of c , T and μ between the model with both helium and metal diffusion and the model without any diffusion. From Fig. 4, we can see that the effect of metal diffusion on the c , T and μ not

only in the convective envelope but also in the radiation interior. Due to diffusion, helium and metal drift inward just below the convection zone and decrease μ in the outer envelope. At the same time, the depletion of Z increase the opacity in the envelope, otherwise the concentration decrease the opacity in the radiation interior. It leads to lower temperature in the envelope and higher value in the interior. From Fig. 4, we can see that the temperature is more sensitive to the metal diffusion than other physical parameters. The $\delta c/c$ is mainly dependent on the variation of $\delta T/T$. Except the convective envelope, the sound speed c is much larger in the interior of the model. From the expression of the sound speed gradient in terms of the equation (16):

$$\frac{dc}{dr} \propto \frac{d(\frac{T}{\mu})^{1/2}}{dr} = -\frac{1}{2}(\frac{T}{\mu^3})^{\frac{1}{2}} \frac{d\mu}{dr} + \frac{1}{2} \frac{1}{(T\mu)^{\frac{1}{2}}} \frac{dT}{dr} \quad (17)$$

we find that the temperature T is the dominate factor in the sound speed gradient in causing the differences between the models with and without metal diffusion. Due to dT/dr is negative, $|dc/dr|$ is larger than that of model without metal diffusion in the radiation interior. So from equation (14), the small spacings are larger than other models. That are explained the variation of the internal structure including metal diffusion.

5 CONCLUSIONS

Taking into account the effects of helium and metal diffusion on stellar evolution, we have presented a detailed modeling of the MOST target: the star ϵ Eridani by fitting the available observational constraints: effective temperature, luminosity, high precision interferometric observational radius and metallicity. We also consider the age (≤ 1 Gyr) as a property of star to constraint the models, which are the same as SD89.

According to our results, the location in the H-R diagram indicates that the star ϵ Eridani has evolved little since its arrival on the zero-age main sequence. Taking into account the helium and metal diffusion, we find that the mean large spacings $< \Delta\nu >$, which are averaged over $l = 0, 1, 2, 3$ and $n = 10, 11, 12, \dots, 30$, is about $194 \pm 1 \mu Hz$.

In order to test the effect of helium and metal diffusion, we construct three groups of models with the same mass but different Y_i and Z_i . Then, for the given chemical composition we calibrate three models with the different types of diffusion which are listed in Table 2. In our work we fixed the mixing length parameter $\alpha = 1.70$ and neglected convective overshoot. The results show that the age of diffused models is about 1 Gyr, and be younger than that determined by the models without diffusion.

Due to the effect of diffusion, helium and metal fall below the outer convective zone and form a gradient. We use the ‘‘second differences’’ to test the depth of the convective zones. When metal diffusion is considered, the convective zone deepens more quickly and the metal gradient steepens more rapidly than the helium gradient. That induce a stronger reflection of the sound waves just below the convection zone, which explains the higher amplitude of the peak related to the base of the convective zone than that of pure helium diffusion.

The small spacings and frequency separation ratios have been used to test the differences of internal structure in models with and without diffusion. According to our results, the pure helium diffusion hardly alter the internal structure in the young low-mass models. Taking into account the metal diffusion, it mainly induce a much higher temperature in the radiation interior, thereby the higher

sound speed in the interior of the model. Correspondingly, the frequencies and large spacings are larger obviously than that of models without metal diffusion. The variation of internal structures between models with and without metal diffusion is increase obviously alone with the increase of initial metallicity. So we conclude that it is necessary to consider the metal diffusion in the young main-sequence low-mass star.

Acknowledgements We are grateful to anonymous referee for his/her constructive suggestions and valuable remarks to improve the manuscript. This work was supported by The Ministry of Science and Technology of the People's republic of China through grant 2007CB815406, and by NSFC grants 10173021, 10433030, 10773003, and 10778601.

References

- Alexander D. R., Ferguson J. W., 1994, *ApJ*, 437, 879
- Bahcall J. N., 1989, *Neutrino Astrophysics*, Cambridge Univ: Cambridge
- Bahcall J. N., Loeb A., 1990, *ApJ*, 360, 267
- Bahcall J. N., Pinsonneault M. H., 1992a, *RvMP*, 64, 885
- Bahcall J. N., Pinsonneault M. H., 1992b, *ApJ*, 395, 119
- Bahcall J. N., Pinsonneault M. H., Wasserburg G. L., 1995, *RvMP*, 67, 781
- Basu S., Chaplin W. J., Elsworth Y. et al., 2007, *ApJ*, 655, 660
- Bi S. L., Basu S., Li L. H., 2008, *ApJ*, 673, 1093
- Burgers J. M., 1969, *Flow equations for composite gases* (New York and London: Academic Press)
- Castro M., Vauclair S., 2006, *A&A*, 456, 611
- Chaboyer B., Deliyannis C. P., Demarque P. et al., 1992, *ApJ*, 388, 372
- Chapman S., Cowling T. G., 1970, *The Mathematical Theory of Non-Uniform Gases*, Cambridge University Press, 3rd edn
- Christensen - Dalsgaard J., Berthomieu G., 1991, in *Solar Interior and Atmosphere*, Thcson, AZ, University of Arizona Press, 1991, 401
- Christensen - Dalsgaard J., Proffitt C. R., Thompson M. J., 1993, *ApJ*, 403, L75
- Cox A. N., Guzik J. A., Kidman R. B., 1989, *ApJ*, 342, 1187
- Di Folco E., Thévenin F., Kervella P. et al., 2004, *A&A*, 426, 601
- Donahue R. A., 1993, Ph.D thesis, New Mexico State Univ.
- Eggenberger P., Carrier F., Bouchy F., 2005, *NewA*, 10, 195
- Fischer D. A., Valenti J., 2005, *ApJ*, 622, 1102
- Gough D. O., 1990, *LNP*, 367, 283
- Grevesse N., Sauval A. J., 1998, *SSRv*, 85, 161
- Guenther D. B., Demarque P., 1986, *ApJ*, 301, 207
- Guenther D. B., 1987, *ApJ*, 312, 211
- Guenther D. B., Pinsonneault M. H., Bahcall J. H., 1993, *ApJ*, 418, 469
- Guenther D. B., 1994, *ApJ*, 422, 400
- Guenther D. B., Demarque P., 1997, *ApJ*, 484, 937
- Hatzes A. P., Cochran W. D., McArthur B. et al., 2000, *ApJ*, 544, 145
- Iglesias C. A., Rogers F. J., 1996, *ApJ*, 464, 943
- Krishna Swamy K. S., 1966, *ApJ*, 145, 174
- Loeb A., Bahcall J. N., Milgrom M., 1989, *ApJ*, 341, 1108

- Murphy E. J., Demarque P., Guenther D. B., 2004, *ApJ*, 605, 472
- Mazumdar A., Antia H. M., 2001, *A&A*, 377, 192
- Michaud G., Charland Y., Vauclair S. et al., 1976, *ApJ*, 210, 447
- Minier V., Lineweaver C., 2006, *A&A*, 449, 805
- Noerdlinger P. D., 1977, *A&A*, 57, 407
- Noyes R. W., Baliunas S. L., Belserene E. et al., 1984, *ApJ*, 285, L23
- Press W. H., Flannery B. P., Teukolsky S. A., 1986, *Numerical Recipes* (Cambridge University, Cambridge, England)
- Proffitt C. R., 1994, *AJ*, 425, 849
- Ramírez I., Meléndez J., 2004, *ApJ*, 609, 417
- Rocha-Pinto H. J., Maciel W. J., 1998, *MNRAS*, 298, 332
- Rogers F. J., Nayfonov A., 2002, *ApJ*, 576, 1064
- Roxburgh I. W., Vorontsov S. V., 2003, *A&A*, 411, 215
- Saffe C., Gómez M., Chavero C., 2005, *A&A*, 443, 609
- Santos N. C., Israelian G., Mayor M., 2001, *A&A*, 373, 1019S
- Santos N. C., Israelian G., Mayor M., 2004, *A&A*, 415, 1153
- Soderblom D. R., Däppen W., 1989, *ApJ*, 342, 945
- Song I., Caillault J. -P., Barrado y Navascués D. et al., 2000, *ApJ*, 533, L41
- Takeda Y., Ohkubo M., Sato B. et al., 2005, *PASJ*, 57, 27
- Tassoul M., 1980, *ApJS*, 43, 469
- Théado S., Vauclair S., Castro M. et al., 2005, *A&A*, 437, 553
- Thoul A. A., Bahcall J. N., Loeb A., 1994, *ApJ*, 421, 828
- Thoul A. A., Scuflaire R., Noels A. et al., 2003, *A&A*, 402, 293
- Vauclair S., Théado S., 2004, *A&A*, 425, 179

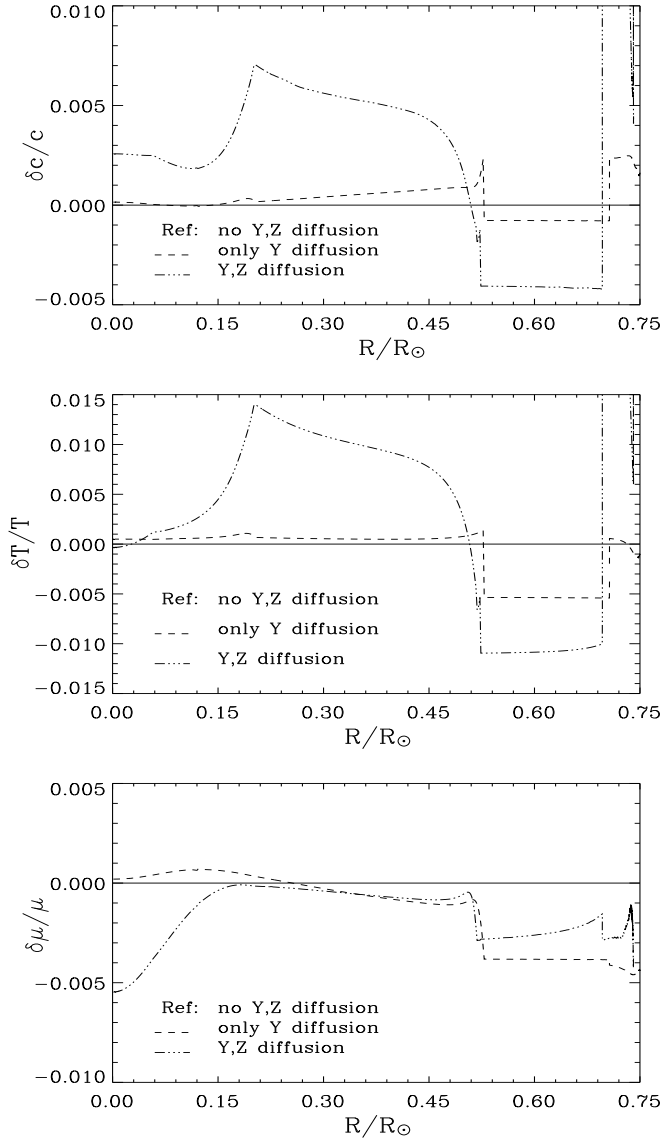


Fig. 4 From up to down, each panel of figure give the relative sound-speed difference $\delta c/c$, the temperature difference $\delta T/T$ and the mean molecular weight $\delta \mu/\mu$ respectively for the models in group (C). All differences are with respect to the model C1 which without any diffusion. The dashed lines render the differences between the model with pure *He* diffusion and the model without any diffusion (e.g. $\delta \mu/\mu = (\mu_{Y.Dif} - \mu_{None.Dif}) / \mu_{None.Dif}$). The dash dot lines render the differences between the model with *He* & *Z* diffusion and the model without any diffusion (e.g. $\delta \mu/\mu = (\mu_{Y\&Z.Dif} - \mu_{None.Dif}) / \mu_{None.Dif}$).